The Astrophysical Journal, 738:104 (8pp), 2011 September 1 doi:10.1088/0004-637X/738/1/104

MEAN-FIELD SOLAR DYNAMO MODELS WITH A STRONG MERIDIONAL FLOW AT THE BOTTOM OF THE CONVECTION ZONE

V. V. Pipin[1,2,3] and A. G. Kosovichev[3]
[1] Institute of Geophysics and Planetary Physics, UCLA, Los Angeles, CA 90065, USA
[2] Institute of Solar-Terrestrial Physics, Russian Academy of Sciences, 664033 Irkutsk, Russia
[3] Hansen Experimental Physics Laboratory, Stanford University, Stanford, CA 94305, USA
Received 2011 April 7; accepted 2011 June 21; published 2011 August 17

ABSTRACT

This paper presents a study of kinematic axisymmetric mean-field dynamo models for the case of meridional circulation with a deep-seated stagnation point and a strong return flow at the bottom of the convection zone. This kind of circulation follows from mean-field models of the angular momentum balance in the solar convection zone. The dynamo models include turbulent sources of the large-scale poloidal magnetic field production due to kinetic helicity and a combined effect due to the Coriolis force and large-scale electric current. In these models the toroidal magnetic field, which is responsible for sunspot production, is concentrated at the bottom of the convection zone and is transported to low-latitude regions by a meridional flow. The meridional component of the poloidal field is also concentrated at the bottom of the convection zone, while the radial component is concentrated in near-polar regions. We show that it is possible for this type of meridional circulation to construct kinematic dynamo models that resemble in some aspects the sunspot magnetic activity cycle. However, in the near-equatorial regions the phase relation between the toroidal and poloidal components disagrees with observations. We also show that the period of the magnetic cycle may not always monotonically decrease with the increase of the meridional flow speed. Thus, for further progress it is important to determine the structure of the meridional circulation, which is one of the critical properties, from helioseismology observations.

Key words: magnetohydrodynamics (MHD) – Sun: dynamo – turbulence

1. INTRODUCTION

The widely accepted paradigm about the nature of global magnetic activity of the Sun assumes that meridional circulation is an important part of the dynamo processes operating in the solar convection zone (Choudhuri et al. 1995; Durney 1995; Choudhuri & Dikpati 1999; Miesch et al. 2010). The current flux-transport and mean-field dynamo models (e.g., Dikpati & Charbonneau 1999; Guerrero & Muñoz 2004; Bonanno et al. 2002) typically employ an analytical profile of the meridional circulation pattern, which has to satisfy a mass conservation equation and the relevant boundary conditions. One of the basic features of this profile is that the circulation stagnation point is close to the middle of the convection zone (e.g., Bonanno et al. 2002; Dikpati et al. 2004). However, such ad hoc models of the meridional flow have no support from the mean-field theory of the angular momentum distribution in the solar convection zone (Kitchatinov & Rüdiger 1999; Kitchatinov & Olemskoy 2011; also see Garaud & Acevedo Arreguin 2009). This theory predicts a meridional circulation pattern with nearly equal amplitudes of the flow velocity at the bottom and top of the convection zone. The stagnation point of this flow is close to the bottom of the convection zone, near $0.75\,R_\odot$, and the circulation is concentrated near the convection zone boundaries. Rempel (2005, 2006) obtained a similar meridional circulation profile with a deep stagnation point and used it to construct a nonlinear dynamo model.

The physical mechanisms of the strong deviation of the meridional circulation pattern from simple analytical models are discussed in the recent paper by Kitchatinov & Olemskoy (2011). Here, we briefly summarize their main arguments. The distribution of large-scale flows in the bulk of the convection zone is close to the Taylor–Proudman balance. However, this balance is violated near the boundaries. This results in a concentration of the circulation velocity in the Eckman layers near the bottom and top of the convection zone (Durney 1999; Miesch et al. 2006; Brun et al. 2010).

Our goal is to investigate how the meridional circulation with a fast return flow at the bottom of the convection zone can affect solar dynamo models. We construct a series of kinematic mean-field dynamo models that employ the meridional circulation pattern suggested by Kitchatinov & Olemskoy (2011). These dynamo models include the turbulent generation of the magnetic field due to the kinetic helicity (α-effect), the combined effect of the Coriolis force and large-scale current ($\Omega \times J$-effect), and the toroidal magnetic field generation due to the differential rotation (Ω-effect). Following Krause & Rädler (1980), these models can be classified as $\alpha^2\delta\Omega$ dynamo models. Our approach is to investigate conditions of the dynamo instability for this type of meridional circulation and determine the basic properties of the dynamo solution at the instability threshold. This is a kinematic dynamo problem. The next section describes the formulation of the mean-field dynamo model, including the basic assumptions, the reference model of the solar convection zone, and input parameters of the large-scale flows. Section 3 presents the results and discussion. The main findings are summarized in Section 4.

2. BASIC EQUATIONS

2.1. Formulation of Model

The dynamo model is based on the standard mean-field induction equation in turbulent perfectly conducting media

(Krause & Rädler 1980):

$$\frac{\partial \mathbf{B}}{\partial t} = \nabla \times (\mathcal{E} + \mathbf{U} \times \mathbf{B}), \quad (1)$$

where $\mathcal{E} = \overline{\mathbf{u} \times \mathbf{b}}$ is the mean electromotive force, with $\mathbf{u}$ and $\mathbf{b}$ being the turbulent fluctuating velocity and magnetic field, respectively; $\mathbf{U}$ is the mean velocity. A general expression for $\mathcal{E}$ was computed by Pipin (2008). Following Krause & Rädler (1980) we write the expression for the mean electromotive force as follows:

$$\mathcal{E}_i = (\alpha_{ij} + \gamma_{ij})\overline{B} - \eta_{ijk}\nabla_j \overline{B}_k, \quad (2)$$

where the tensor $\alpha_{i,j}$ represents the turbulent α-effect, the tensor $\gamma_{i,j}$ describes the turbulent pumping, and the term η_{ijk} describes the anisotropic diffusion due to the Coriolis force and the $\Omega \times J$-effect (Rädler 1969). It is known that a solar-type dynamo model cannot be constructed only with the α-effect as the prime turbulent source of the poloidal magnetic field generation (Stix 1976; Pipin & Seehafer 2009; Seehafer & Pipin 2009). The exact mechanism of the large-scale poloidal magnetic field production on the Sun is not known. After Parker (1955), it is believed that the α-effect (associated with cyclonic convection) is the most important turbulent source of the poloidal magnetic field generation on the Sun. In addition, the mean-field theory predicts the magnetic field generation effects due to the interaction of the Coriolis force ($\Omega \times J$-effect) with a large-scale electric current (see Rädler 1969; Krause & Rädler 1980; Rogachevskii & Kleeorin 2003).

We consider a large-scale axisymmetric magnetic field, $\bar{\mathbf{B}} = \mathbf{e}_\phi B + \nabla \times \frac{A\mathbf{e}_\phi}{r \sin\theta}$, where $B(r, \theta, t)$ is the azimuthal component of the magnetic field, $A(r, \theta, t)$ is proportional to the azimuthal component of the vector potential, r is the radial coordinate, and θ is the polar angle. The mean flow is given by the velocity vector $\mathbf{U} = \mathbf{e}_r U_r + \mathbf{e}_\theta U_\theta + \mathbf{e}_\phi r \sin\theta \Omega$, where $\Omega(r, \theta)$ is the angular velocity of the solar differential rotation, and $U_r(r, \theta)$ and $U_\theta(r, \theta)$ represent the velocity components of the meridional circulation. The mean-field magnetic field evolution is governed by the dynamo equations, which follow from Equation (1):

$$\frac{\partial A}{\partial t} = r \sin\theta \mathcal{E}_\phi + \frac{U_\theta \sin\theta}{r}\frac{\partial A}{\partial \mu} - U_r \frac{\partial A}{\partial r} \quad (3)$$

$$\frac{\partial B}{\partial t} = -\frac{\sin\theta}{r}\left(\frac{\partial \Omega}{\partial r}\frac{\partial A}{\partial \mu} - \frac{\partial \Omega}{\partial \mu}\frac{\partial A}{\partial r}\right) - \frac{\partial (r U_r B)}{\partial r} + \frac{\sin\theta}{r}\frac{\partial U_\theta B}{\partial \mu} + \frac{1}{r}\frac{\partial r \mathcal{E}_\theta}{\partial r} + \frac{\sin\theta}{r}\frac{\partial \mathcal{E}_r}{\partial \mu}. \quad (4)$$

We introduce the free parameter C_η to control the turbulent diffusion coefficient (see the Appendix) and the free parameters C_α and $C_\delta^{(\Omega)}$ to control the strengths of the α- and $\Omega \times J$-effects.

We use the solar convection zone model computed by Stix (2002) for the mixing-length parameter $\alpha_{\rm MLT} \equiv \ell |\mathbf{\Lambda}^{(p)}| = 2$, where ℓ is the mixing length and $\mathbf{\Lambda}^{(p)} = \nabla \log \overline{p}$ is the inverse pressure scale height. We confine the integration domain between $0.712\, R_\odot$ and $0.972\, R_\odot$ in radius. It extends from pole to pole in latitude. The differential rotation profile, $\Omega = \Omega_0 f_\Omega(x, \mu)$, where $x = r/R_\odot$ and $\mu = \cos\theta$, is a modified version of the analytical approximation of helioseismology data proposed by Antia et al. (1998). The model includes part of the rotational shear layer at the bottom of the convection zone, the so-called tachocline (Figure 1(a)). The turbulent diffusivity, $\eta_T^{(0)}$, has a large gradient in this layer (Figure 1(d)). The bottom boundary condition is set where the turbulent diffusivity vanishes according to Stix's model. The convective overshoot region is not included in our model. The dynamo does not operate in this region, but magnetic flux tubes can be stored there until they reach the necessary amplification to become buoyantly unstable (Guerrero & de Gouveia Dal Pino 2007). This instability is beyond the scope of our paper.

Table 1
The Coefficients for the Meridional Circulation Profile Components Given by Equations (5) and (6)

n	0	1	2	3
$c_\theta^{(n)}$	−0.13432(5)	−0.40473(6)	−0.02170(3)	−0.10718(5)
$c_r^{(n)}$	−0.0681469(4)	−0.006839(4)	−0.032516(1)	−0.0027(4)

The meridional flow is modeled in the form of two stationary circulation cells, one in the northern and one in the southern hemisphere, with a poleward motion in the upper and an equatorward motion in the lower part of the convection zone. Following Kitchatinov & Olemskoy (2011), the meridional circulation velocity components are approximated via the orthogonal Chebyshev polynomial decompositions:

$$U_\theta = 3U_0 \sin\theta \cos\theta \sum_{n=0}^{3} c_\theta^{(n)} T_n(\xi), \quad (5)$$

$$U_r = U_0(3\cos^2\theta - 1)(1 - \xi^2)\sum_{n=0}^{3} c_r^{(n)} T_n(\xi), \quad (6)$$

where

$$\xi = \frac{2x - x_e - x_b}{x_e - x_b}. \quad (7)$$

Here, $x_{b,e}$ are the radial boundaries of the integration domain. In our case, $x_b = 0.712$ and $x_e = 0.972$. The coefficients $c_\theta^{(n)}$ and $c_r^{(n)}$ are given in Table 1. The parameter U_0 controls the speed of the meridional circulation. Kitchatinov & Olemskoy (2011) obtain $U_0 \approx 16$ m s^{-1}.

The geometry of the meridional flow is illustrated in Figure 1(b). Figure 1(c) shows the latitudinal component of the circulation in units of U_0.

The boundary conditions represent a perfect conductor at the bottom and the potential magnetic field configuration outside the domain.

2.2. Method of Solution

We investigate the linear stability of the dynamo equations (3) and (4) and determine unstable dynamo modes. Then we construct linear dynamo solutions using the corresponding eigenfunctions. Our approach to solving the linear problem was described in detail by Pipin & Seehafer (2009) and Seehafer & Pipin (2009). We use a Galerkin method, expanding the magnetic field in terms of a basis that satisfies the boundary conditions (Boyd 2001; Livermore & Jackson 2005). The system of Equations (3) and (4) has exponentially growing or decaying solutions, which we represent in the form

$$A(x, \theta, t) = e^{\sigma t} \sum_n \sum_m A_{nm} \sin\theta\, S_{nm}^{(A)}(\xi) P_m^1(\cos\theta), \quad (8)$$

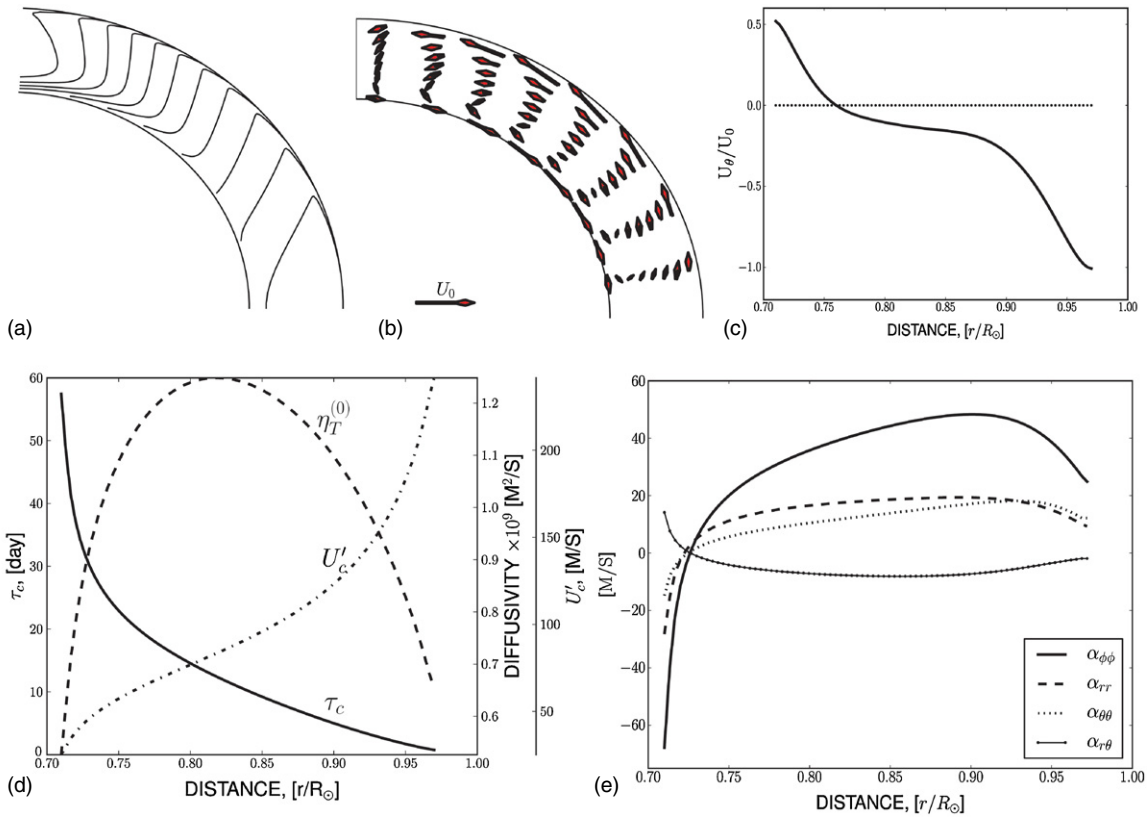

Figure 1. Internal parameters of the solar convection zone: (a) the contours of angular velocity are plotted for the levels $(0.75–1.05)\Omega_0$ with a step of $0.025\Omega_0$, $\Omega_0 = 2.86 \times 10^{-7}$ s^{-1}; (b) the vector field of the meridional circulation with $|\mathbf{U}|$ measured in units of U_0; (c) the meridional component of circulation at $\theta = 45^\circ$; (d) turnover convection time τ_c, the background turbulent diffusivity $\eta_T^{(0)}$, and rms convective velocity U_c'; and (e) the radial profiles of the α-effect components at $\theta = 45^\circ$.

$$B(x, \theta, t) = \mathrm{e}^{\sigma t} \sum_n \sum_m B_{nm} S_n^{(B)}(\xi) P_m^1(\cos\theta), \qquad (9)$$

where $S_{nm}^{(A)}(\xi)$ and $S_n^{(B)}(\xi)$ are linear combinations of Legendre polynomials, and P_m^1 is the associated Legendre function of degree m and order 1. These expansions ensure the regularity of the solutions at the poles $\theta = 0$ and $\theta = \pi$. The integrations in radius and latitude, which are needed for calculating the expansion coefficients A_{nm} and B_{nm}, are done by means of the Gauss–Legendre procedure. The eigenvalue problem for determining the eigenvalues, σ, and the associated eigenfunctions is solved by using the LAPACK software. There are two types of dynamo eigenmodes: (1) modes with a symmetric distribution of the toroidal component B and antisymmetric distribution of the poloidal component A, relative to the equator, called here "S-modes," and (2) vice versa, modes with antisymmetric A and symmetric B, called "A-modes." We define the eigenvalues of the S- and A-modes as $\sigma^{(S)} = \lambda^{(S)} + i\omega^{(S)}$ and $\sigma^{(A)} = \lambda^{(A)} + i\omega^{(A)}$, respectively. The spectral resolution of our calculations was 16 radial and 25 latitudinal basis functions. The results are qualitatively confirmed by a number of runs with a larger number of basis functions.

3. RESULTS

We calculate the dynamo solutions for a relatively low level of the background turbulent diffusivity, choosing $C_\eta = 0.1$, in order to approximately match the period of the eigenmodes with the solar cycle period. This corresponds to the maximum background diffusivity $\sim 10^8$ m^2 s^{-1}. Figure 2 (left column) shows the linear stability diagrams for the dynamo models with meridional circulation speed values equal to $U_0 = 8, 12$, and 16 m s^{-1}. The growth rate $\lambda^{(A)} = Re(\sigma^{(A)})$ of the first, most unstable, dynamo mode (A-mode) is shown by the gray-scale plots in the (C_α, C_δ) plane, where C_α and C_δ are the free parameters that control the strength of the α- and $\Omega \times J$-effects. We find that the dynamo instability region (represented by white color) changes significantly with the increase in the meridional circulation speed. For the slow meridional circulation, it is found that the first A-mode is stable and steady in the absence of the α-effect ($C_\alpha = 0$). It has an excitation threshold of $C_\delta \approx 0.013$. In the opposite limit, when $C_\delta = 0$, the first mode is stable and oscillating. Its oscillation frequency grows with the increase in the α-effect parameter C_α. The excitation threshold is $C_\alpha \approx 0.025$. The oscillation frequency of the mode at the threshold is about $8\eta_T^{(0)}/R_\odot^2$.

The right column in Figure 2 shows the growth rate of the first A-mode relative to the first S-mode. The relative difference is characterized by the parameter $\Delta\lambda/\lambda = (|\lambda^{(A)}| - |\lambda^{(S)}|)/(|\lambda^{(A)}| + |\lambda^{(S)}|)$. This helps to identify the regions in the parameter space (C_α, C_δ) where the A-mode dominates the S-mode. We find that in the case of $U_0 = 8$ m s^{-1} the A-mode is dominant for $C_\alpha \geqslant C_\delta$. In this regime we look for a solar-type dynamo solution, because in the solar dynamo the toroidal magnetic field is of A-type (antisymmetric relative to the equator).

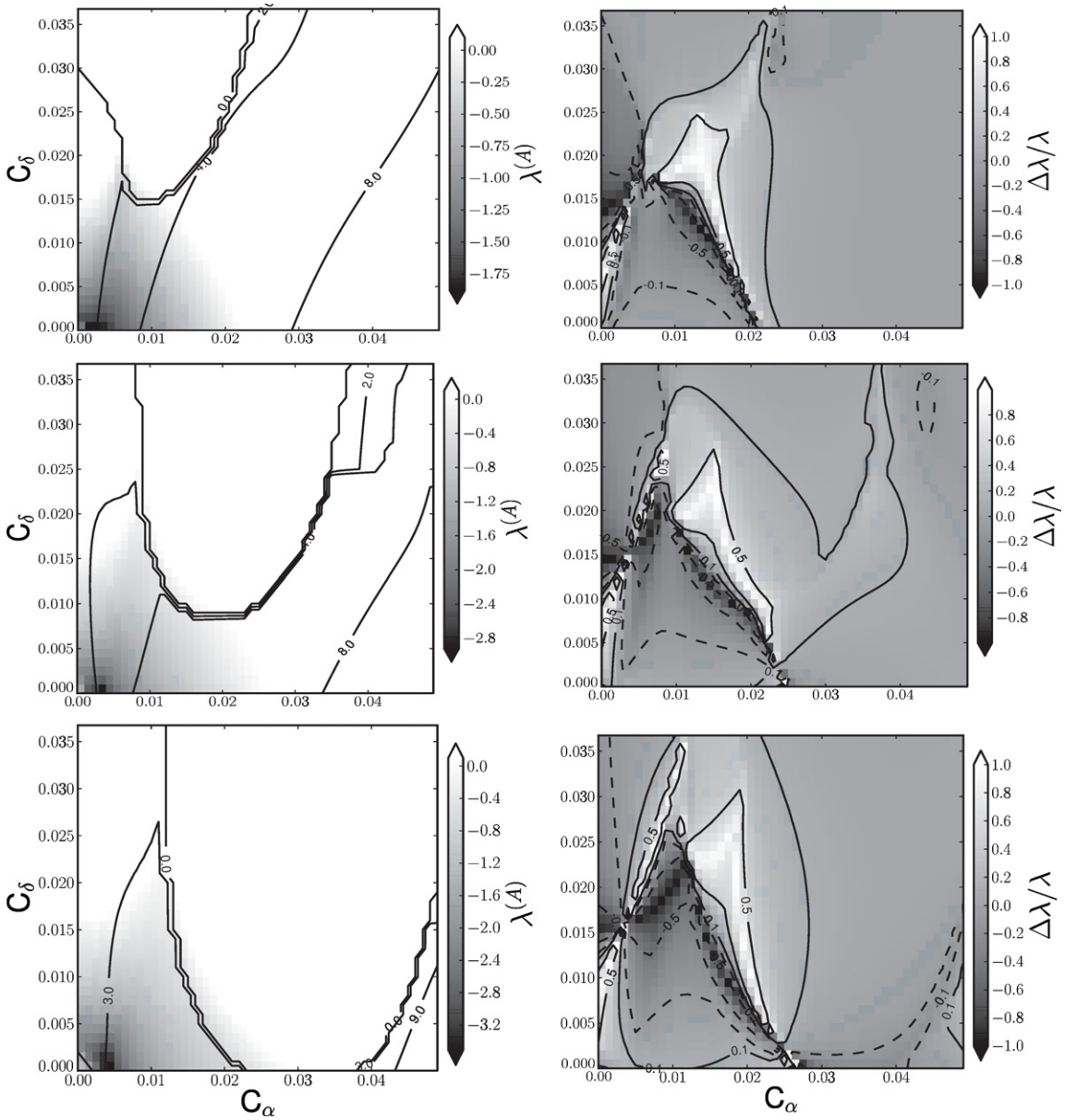

Figure 2. Left column shows the linear stability diagrams for the dynamo models with meridional circulation speed $U_0 = 8$, 12, and 16 m s^{-1}, from the top to the bottom panel. The gray scale shows the growth rate of the most unstable A-mode, $\lambda^{(A)}$. The contours show the oscillation frequency, $\omega^{(A)}$, of this mode in units of $\eta_T^{(0)}/R_\odot^2$. Right column shows the relative growth rates of the corresponding A- and S-modes: $\frac{\Delta\lambda}{\lambda} = \frac{|\lambda^{(A)}|-|\lambda^{(S)}|}{|\lambda^{(A)}|+|\lambda^{(S)}|}$, where the S-mode represents a dynamo solution with the toroidal field symmetrical relative to the equator, and the A-mode has the antisymmetric toroidal field. The A-mode dominates in the regions colored in white.

As an example, we examine the case of $C_\delta = 0$, $C_\alpha \approx 0.025$ when the first A-mode has frequency $\approx 8\eta_T^{(0)}/R_\odot^2$. Figure 3 shows the snapshots of the magnetic field variation inside the convection zone (top) and the time–latitude "butterfly" diagram for this mode (bottom). The snapshots show that the toroidal magnetic field is concentrated at the bottom of the convection zone, and the poloidal field is concentrated in the polar regions. Also, the toroidal magnetic field is globally distributed in the bulk of the convection zone. The maximum of the toroidal field distribution drifts to the equator at the bottom of the convection zone and moves to the pole near the surface. The bottom panel of Figure 3 shows the butterfly diagrams of the toroidal field at the bottom of the convection zone (gray-scale background) and of the radial magnetic fields at the surface (contour lines). The toroidal magnetic field evolution pattern has the polar and equatorial branches. The equatorial branch is strongly concentrated in the equator. The phase relation between the radial magnetic field in the polar regions and the toroidal field in the equatorial regions is in agreement with observations of the polar magnetic field and the sunspot butterfly diagram, assuming that sunspots are formed by the emerging toroidal magnetic field. However, this dynamo mode lacks the equatorial branch of the large-scale radial magnetic field, which is also found in observations. The period of the dynamo is about 12 years. This is half the period of the solar magnetic cycle. The period can be increased by further decreasing the diffusivity parameter C_η by a factor of two ($C_\eta \approx 0.05$). However, this leads to a decrease of the excitation threshold and an increase of the effective magnetic Reynolds number ($R_M = U_0 R_\odot/\eta_T$). This means that the S-mode becomes

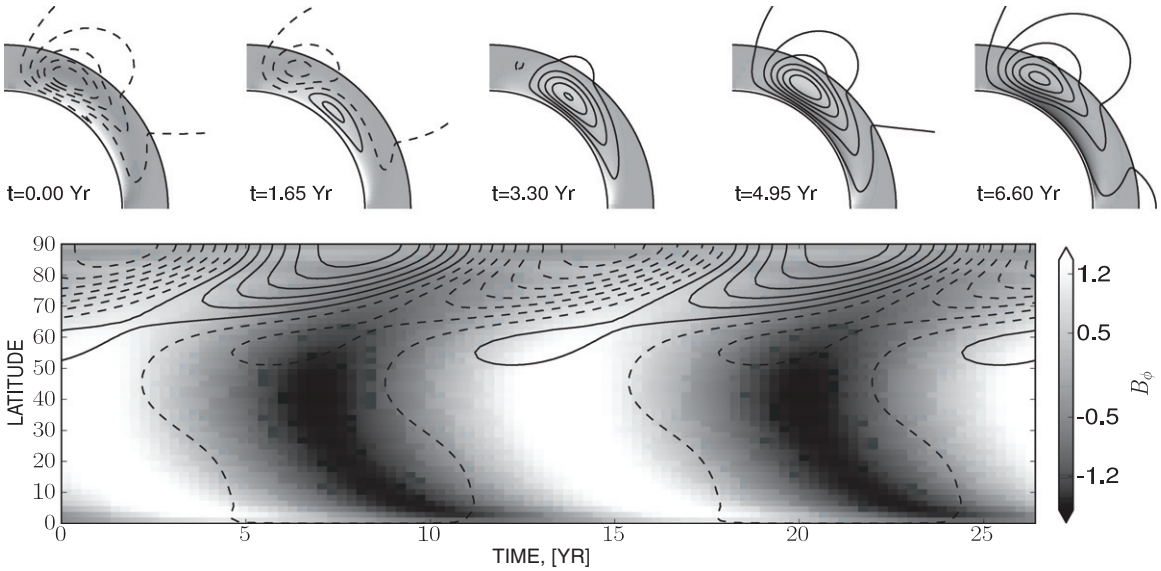

Figure 3. Evolution of the magnetic field (shown in non-dimensional units) in the dynamo model with meridional flow speed $U_0 = 8$ m s^{-1} and $C_\alpha = 0.025$ and $C_\delta = 0$. Top: the snapshots for the magnetic field variations inside the convection zone. The gray-scale background shows distributions of the large-scale toroidal field and contours show the poloidal field lines. Bottom: the time–latitude ("butterfly") diagram for the toroidal magnetic field at the bottom of the convection zone is shown by the gray-scale density plot. The radial field that varies within ± 0.08 (in non-dimensional units) is shown by contours.

dominant, and the solution no longer corresponds to the solar dynamo. Figure 2 shows that for the case of $U_0 = 16$ m s^{-1} the S-mode dominates.

Inspecting the results in Figure 3, we can conclude that the increase in the meridional circulation speed has two main effects on the dynamo instability. First, the larger the U_0, the larger the unstable area in the (C_α, C_δ) space, occupied by the first unstable A-mode (associated with a non-oscillating dynamo solution). Second, the S-mode becomes dominant near the instability threshold everywhere, both for the case of $C_\delta = 0$ and arbitrary C_α and for the case of arbitrary C_δ and $C_\alpha = 0$. The combination of the α- and $\Omega \times J$-effects can make the A-mode dominant, but it represents a non-oscillating dynamo solution.

In another example, we examine the model when the poloidal field is generated both by the α-effect and the $\Omega \times J$-effect, e.g., $C_\alpha = C_\delta = 0.015$ and $U_0 = 8$ m s^{-1}. The oscillation frequency of the first unstable A-mode is about $4\eta_T^{(0)}/R_\odot^2$. Near the excitation threshold, the A-mode is highly dominant over the first S-mode. Figure 4 shows the snapshots of the magnetic field variations inside the convection zone (top) and the butterfly diagram for this mode (bottom). The snapshots of the magnetic field evolution inside the convection zone are similar to those in the previous case. However, the toroidal magnetic field is more strongly concentrated at the bottom of the convection zone, and the polar branch of the toroidal magnetic field evolution is weaker near the surface. The period of the dynamo wave is about 24 years, close to the solar cycle. Generally, we see a significantly better agreement with observations here than seen in the previous case.

In Figure 5 the dependence of the dynamo wave period on the speed of the meridional flow along the stability threshold is shown. Contrary to previous results (e.g., Bonanno et al. 2002; Seehafer & Pipin 2009) the period is not a monotonic function of the flow velocity. The main reason is that here we use the meridional circulation with a different depth dependence. We confirm how the results presented may depend on the distribution of the α-effect. For this, we switched off the effects of the turbulent mixing stratification, making $\Lambda^{(u)} = 0$ in Equation (A1). The dynamo period as a function of the meridional flow speed for this case is shown in Figure 5 (right). We find that the dependence of the dynamo period on the flow speed is much stronger in the case $\Lambda^{(u)} = 0$ for both types of dynamos.

4. DISCUSSION AND CONCLUSIONS

We have studied kinematic axisymmetric mean-field dynamo models for a meridional circulation pattern with a deep-seated stagnation point. This kind of circulation is suggested by the mean-field models of the angular momentum balance in the solar convection zone. We show that by adjusting the turbulent sources of the poloidal magnetic field generation and the turbulent diffusion strength, it is possible to construct a mean-field dynamo model that resembles in some aspects the solar magnetic cycle. The most important features of the investigated models are the following.

The maximum strength of the toroidal magnetic field, which is believed to be responsible for sunspot production, is concentrated near the bottom of the convection zone. This field is transported to the equatorial regions by the meridional flow. The meridional component of the poloidal field is also concentrated at the bottom of the convection zone. The large-scale radial field is concentrated near the poles. It reverses sign when the maximum of the toroidal field gets close to the equator. This is not quite consistent with solar observations, which show that the polar field reversals happen earlier in the cycle. A similar result is demonstrated in the kinematic flux-transport model by Rempel (2006). His model has a qualitatively similar meridional circulation pattern, and the speed at the bottom of the convection zone is half that in our case. We believe that this feature (the phase relation) is inherent for this type of meridional flow, which produced a conveyor-belt-like circulation of the magnetic field (Dikpati et al. 2004). The equatorward and poleward conveyor bands are not well connected in our case because circulation is quite weak in the bulk of the convection zone.

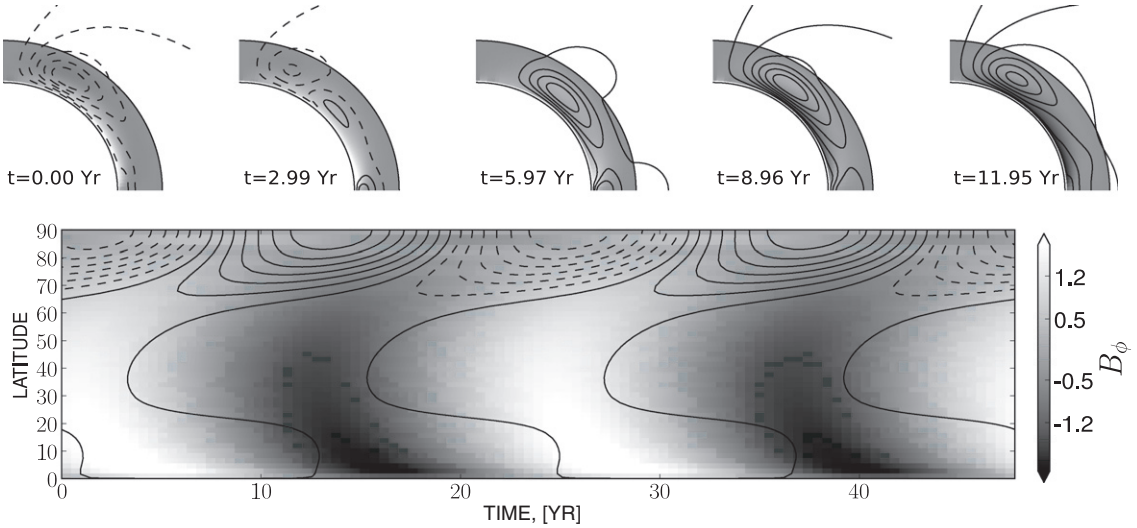

Figure 4. Same as Figure 3 for a dynamo with $C_\alpha = C_\delta = 0.015$. In the butterfly diagram, the radial magnetic field at the surface varies within ± 0.035, and the toroidal field varies within ± 2 (in non-dimensional units).

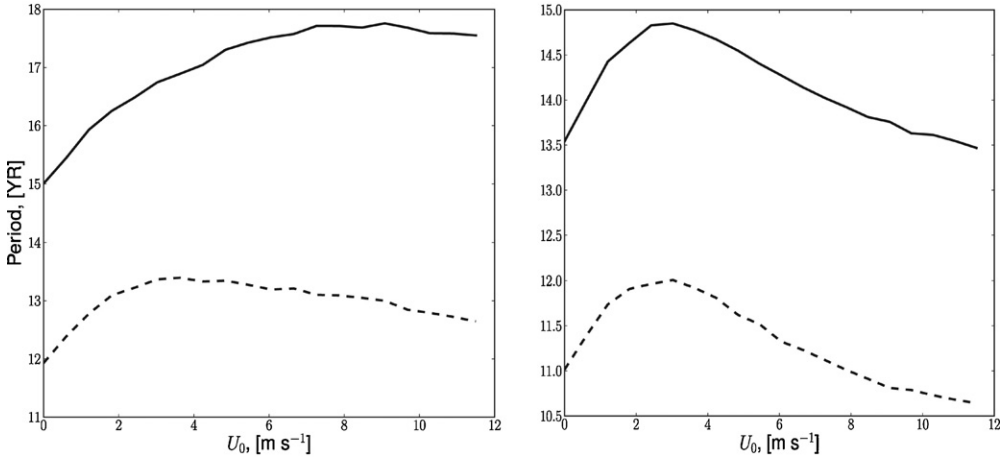

Figure 5. Dependence of the dynamo period on the meridional flow speed U_0 along the stability boundary of the most unstable dipolar mode for the dynamo models with the $\Omega \times J$-effect (solid line) and without it (dashed line). Left: results for a complete α-effect. Right: results for the α-effect without turbulence stratification, $\Lambda^{(u)} = 0$ (see Equation (A1)).

We find that including the combined action of the α- and $\Omega \times J$-effects for the poloidal magnetic field generation improves the agreement of the basic properties of the model with observations. Compared to the standard $\alpha\Omega$ dynamo, the inclusion of the $\Omega \times J$-effect increases the cycle period and the ratio between the maximum of the toroidal magnetic field strength and the strength of the large-scale radial magnetic field in the polar regions. Furthermore, in the model with the $\Omega \times J$-effect, the large-scale toroidal field comes closer to the equator. The toroidal magnetic field in the equatorial branch of the "butterfly" diagram is much stronger than the toroidal field in the polar branch. These properties bring the models with the $\Omega \times J$-effect into better agreement with observations. The linear stability diagrams show that for unstable modes the growth rate of the A-mode (antisymmetric toroidal field relative to the equator) over the S-mode (symmetric mode) is generally higher when the $\Omega \times J$-effect is included. This fact can be invoked to explain the dominance of the antisymmetric toroidal fields in the solar cycle.

Our models show a strong concentration of the toroidal field in the bottom of the convection zone. How this type of dynamo can operate with regard to the magnetic buoyancy effects (Parker 1984) and nonlinear effects due to magnetic helicity conservation (Brandenburg & Subramanian 2005) must be checked by nonlinear model calculations. In our linear models, we cannot give the amplitude of the magnetic field strength in Gauss but we can estimate the ratio between the strength of the toroidal and poloidal components of the large-scale magnetic field. In the model with the $\Omega \times J$-effect (case $C_\alpha = C_\delta = 0.015$), we found that this ratio is about 60.

Contrary to the usual expectations that come from the results of the flux-transport dynamo model, we find that the period of the dynamo cycle does not always become shorter when the speed of the meridional circulation increases. In our model, this rule works for flow amplitude greater than 3 m s^{-1} in the case of the $\alpha^2\Omega$ dynamo with the α-effect dependent on the density stratification, and for flow amplitude greater than 8 m s^{-1} in the case of the $\alpha^2\delta\Omega$ dynamo (which includes the $\Omega \times J$-effect) with the α-effect dependent on both the density and the turbulent diffusivity stratification. The dependence of the dynamo period on the flow amplitude is much stronger if the α-effect does not depend on the turbulence intensity stratification ($\Lambda^{(u)} = 0$).

Thus, by measuring the distributions of the magnetic activity and meridional circulation characteristics on the Sun and

possibly on other cool stars, we may get indirect information about the contribution of the $\Omega \times J$-effect to the dynamo as well as about the relative contributions to the α-effect due to density and turbulent diffusivity stratifications.

We conclude that the meridional flow pattern and speed have to be considered among the most important constraints on the stellar dynamo. Our results show the possibility of using helioseismic observations of the meridional circulation for the diagnostics of the solar dynamo, because the dynamo properties depend significantly on the depth of the flow stagnation point.

This work was supported by NASA LWS TR&T grants NNX09AJ85G and NNX09AT36G, and partially by RFBR grant 10-02-00148-a.

APPENDIX

Here we describe the components of the mean electromotive force that are used in the model. The tensor $\alpha_{i,j}$ represents the turbulent α-effect, and in accordance with Pipin (2008) it is given by

$$\begin{aligned}\alpha_{ij} &= \delta_{ij}\left\{3\eta_T\left(f_{10}^{(a)}(\mathbf{e}\cdot\mathbf{\Lambda}^{(\rho)}) + f_{11}^{(a)}(\mathbf{e}\cdot\mathbf{\Lambda}^{(u)})\right)\right\}\\ &+ e_i e_j\left\{3\eta_T\left(f_{5}^{(a)}(\mathbf{e}\cdot\mathbf{\Lambda}^{(\rho)}) + f_{4}^{(a)}(\mathbf{e}\cdot\mathbf{\Lambda}^{(u)})\right)\right\}\\ &+ 3\eta_T\left\{\left(e_i\Lambda_j^{(\rho)} + e_j\Lambda_i^{(\rho)}\right)f_6^{(a)} + \left(e_i\Lambda_j^{(u)} + e_j\Lambda_i^{(u)}\right)f_8^{(a)}\right\}.\end{aligned} \tag{A1}$$

The tensor $\gamma_{i,j}$ describes the turbulent pumping

$$\begin{aligned}\gamma_{ij} &= 3\eta_T\left\{f_3^{(a)}\Lambda_n^{(\rho)} + f_1^{(a)}(\mathbf{e}\cdot\mathbf{\Lambda}^{(\rho)})e_n\right\}\\ &\times \varepsilon_{inj} - 3\eta_T f_1^{(a)} e_j \varepsilon_{inm} e_n \Lambda_m^{(\rho)},\end{aligned} \tag{A2}$$

and the term η_{ijk} describes the anisotropic diffusion due to the Coriolis force and the $\Omega \times J$-effect (Rädler 1969),

$$\eta_{ijk} = 3\eta_T\left\{\left(2f_1^{(a)} - f_1^{(d)}\right)\varepsilon_{ijk} - 2f_1^{(a)}e_i e_n \varepsilon_{njk} + f_4^{(d)}\delta_{ij}e_k\right\}. \tag{A3}$$

The functions $f_{\{1-11\}}^{(a,d)}$ (given below) depend on the Coriolis number $\Omega^* = 2\tau_c\Omega_0$, and the typical convective turnover time in the mixing-length approximation is $\tau_c = \ell/u'$. The turbulent diffusivity is parameterized in the form $\eta_T = C_\eta \eta_T^{(0)}$, where $\eta_T^{(0)} = \frac{u'\ell}{3}$ is the characteristic mixing-length turbulent diffusivity, u' is the rms convective velocity, ℓ is the mixing length, and C_η is a constant to control the intensity of turbulent mixing. The background turbulence is a state of turbulent flows in the absence of the mean magnetic fields and global rotation. The other quantities in Equations (A1), (A2), and (A3) are as follows: $\mathbf{\Lambda}^{(\rho)} = \nabla \log\overline{\rho}$ is the density stratification scale, $\mathbf{\Lambda}^{(u)} = \nabla \log(\eta_T^{(0)})$ is the scale of turbulent diffusivity, and $\mathbf{e} = \mathbf{\Omega}/|\Omega|$ is a unit vector along the axis of rotation. Equations (A1), (A2), and (A3) take into account the influence of the fluctuating small-scale magnetic fields which can be present in the background turbulence (see discussions in Frisch et al. 1975; Moffatt 1978; Vainshtein & Kitchatinov 1983; Kleeorin et al. 1996; Brandenburg & Subramanian 2005). In our paper, the parameter $\varepsilon = \frac{\overline{\mathbf{b}^2}}{\mu_0\overline{\rho}\overline{\mathbf{u}^2}}$, which measures the ratio between the magnetic and kinetic energies of fluctuations in the background turbulence, is assumed to be equal to 1. This corresponds to energy equipartition.

Below, we give the functions of the Coriolis number defining the dependence of the turbulent transport generation and diffusivities on the angular velocity:

$$f_1^{(a)} = \frac{1}{4\Omega^{*2}}\left((\Omega^{*2}+3)\frac{\arctan\Omega^*}{\Omega^*} - 3\right),$$

$$f_3^{(a)} = \frac{1}{4\Omega^{*2}}\left(((\varepsilon-1)\Omega^{*2}+\varepsilon-3)\frac{\arctan\Omega^*}{\Omega^*} + 3 - \varepsilon\right),$$

$$\begin{aligned}f_4^{(a)} = \frac{1}{6\Omega^{*3}}&\left(3(\Omega^{*4}+6\varepsilon\Omega^{*2}+10\varepsilon-5)\frac{\arctan\Omega^*}{\Omega^*}\right.\\ &\left.-((8\varepsilon+5)\Omega^{*2}+30\varepsilon-15)\right),\end{aligned}$$

$$\begin{aligned}f_5^{(a)} = \frac{1}{3\Omega^{*3}}&\left(3(\Omega^{*4}+3\varepsilon\Omega^{*2}+5(\varepsilon-1))\frac{\arctan\Omega^*}{\Omega^*}\right.\\ &\left.-((4\varepsilon+5)\Omega^{*2}+15(\varepsilon-1))\right),\end{aligned}$$

$$\begin{aligned}f_6^{(a)} = -\frac{1}{48\Omega^{*3}}&\left(3((3\varepsilon-11)\Omega^{*2}+5\varepsilon-21)\frac{\arctan\Omega^*}{\Omega^*}\right.\\ &\left.-(4(\varepsilon-3)\Omega^{*2}+15\varepsilon-63)\right),\end{aligned}$$

$$\begin{aligned}f_8^{(a)} = -\frac{1}{12\Omega^{*3}}&\left(3((3\varepsilon+1)\Omega^{*2}+4\varepsilon-2)\frac{\arctan\Omega^*}{\Omega^*}\right.\\ &\left.-(5(\varepsilon+1)\Omega^{*2}+12\varepsilon-6)\right),\end{aligned}$$

$$\begin{aligned}f_{10}^{(a)} = -\frac{1}{3\Omega^{*3}}&\left(3(\Omega^{*2}+1)(\Omega^{*2}+\varepsilon-1)\frac{\arctan\Omega^*}{\Omega^*}\right.\\ &\left.-((2\varepsilon+1)\Omega^{*2}+3\varepsilon-3)\right),\end{aligned}$$

$$\begin{aligned}f_{11}^{(a)} = -\frac{1}{6\Omega^{*3}}&\left(3(\Omega^{*2}+1)(\Omega^{*2}+2\varepsilon-1)\frac{\arctan\Omega^*}{\Omega^*}\right.\\ &\left.-((4\varepsilon+1)\Omega^{*2}+6\varepsilon-3)\right).\end{aligned}$$

$$\begin{aligned}f_1^{(d)} = &\frac{1}{2\Omega^{*3}}\\ &\times\left((\varepsilon+1)\Omega^{*2}+3\varepsilon-((2\varepsilon+1)\Omega^{*2}+3\varepsilon)\frac{\arctan(\Omega^*)}{\Omega^*}\right),\end{aligned}$$

$$f_4^{(d)} = \frac{1}{2\Omega^{*3}}\left((2\Omega^{*2}+3) - 3(\Omega^{*2}+1)\frac{\arctan(\Omega^*)}{\Omega^*}\right).$$

REFERENCES

Antia, H. M., Basu, S., & Chitre, S. M. 1998, MNRAS, 298, 543
Bonanno, A., Elstner, D., Rüdiger, G., & Belvedere, G. 2002, A&A, 390, 673
Boyd, J. 2001, Chebyshev and Fourier Spectral Methods (2nd ed., New York: Dover), 688
Brandenburg, A., & Subramanian, K. 2005, Phys. Rep., 417, 1
Brun, A. S., Antia, H. M., & Chitre, S. M. 2010, A&A, 510, A33
Choudhuri, A. R., & Dikpati, M. 1999, Sol. Phys., 184, 61
Choudhuri, A. R., Schussler, M., & Dikpati, M. 1995, A&A, 303, L29
Dikpati, M., & Charbonneau, P. 1999, ApJ, 518, 508
Dikpati, M., de Toma, G., Gilman, P. A., Arge, C. N., & White, O. R. 2004, ApJ, 601, 1136
Durney, B. R. 1995, Sol. Phys., 160, 213
Durney, B. R. 1999, ApJ, 511, 945
Frisch, U., Pouquet, A., Léorat, J., & Mazure, A. 1975, J. Fluid Mech., 68, 769
Garaud, P., & Acevedo Arreguin, L. 2009, ApJ, 704, 1
Guerrero, G. A., & de Gouveia Dal Pino, E. M. 2007, Astron. Nachr., 328, 1122

Guerrero, G. A., & Muñoz, J. D. 2004, MNRAS, 350, 317
Kitchatinov, L. L., & Olemskoy, S. V. 2011, MNRAS, 411, 1059
Kitchatinov, L. L., & Rüdiger, G. 1999, A&A, 344, 911
Kleeorin, N., Mond, M., & Rogachevskii, I. 1996, A&A, 307, 293
Krause, F., & Rädler, K.-H. 1980, Mean-Field Magnetohydrodynamics and Dynamo Theory (Berlin: Akademie-Verlag)
Livermore, P. W., & Jackson, A. 2005, Geophys. Astrophys. Fluid Dyn., 99, 467
Miesch, M. S., Brown, B. P., Browning, M. K., Brun, A. S., & Toomre, J. 2010, arXiv:1009.6184
Miesch, M. S., Brun, A. S., & Toomre, J. 2006, ApJ, 641, 618
Moffatt, H. K. 1978, Magnetic Field Generation in Electrically Conducting Fluids (Cambridge: Cambridge Univ. Press)
Parker, E. N. 1955, ApJ, 122, 293
Parker, E. N. 1984, ApJ, 281, 839
Pipin, V. V. 2008, Geophys. Astrophys. Fluid Dyn., 102, 21
Pipin, V. V., & Seehafer, N. 2009, A&A, 493, 819
Rädler, K.-H. 1969, Monats. Dt. Akad. Wiss., 11, 194
Rempel, M. 2005, ApJ, 622, 1320
Rempel, M. 2006, ApJ, 647, 662
Rogachevskii, I., & Kleeorin, N. 2003, Phys. Rev. E, 68, 1
Seehafer, N., & Pipin, V. V. 2009, A&A, 508, 9
Stix, M. 1976, A&A, 47, 243
Stix, M. 2002, The Sun: An Introduction (2nd ed.; Berlin: Springer)
Vainshtein, S. I., & Kitchatinov, L. L. 1983, Geophys. Astrophys. Fluid Dyn., 24, 273